Hindawi
Adsorption Science & Technology
Volume 2022, Article ID 7195777, 17 pages
https://doi.org/10.1155/2022/7195777

Research Article

Pb (II) Recovery by Modified Tuffite: Adsorption, Desorption, and Kinetic Study

Beyhan Kocadagistan[1] **and Kubra Oksuz**[2]

[1]*Ataturk University, Engineering Faculty, Environmental Engineering Department, 25240 Erzurum, Turkey*
[2]*Ataturk University, Natural and Applied Sciences Graduate School, Environmental Engineering Department, 25240 Erzurum, Turkey*

Correspondence should be addressed to Beyhan Kocadagistan; beyhank@atauni.edu.tr

Received 29 March 2022; Revised 1 July 2022; Accepted 1 August 2022; Published 13 August 2022

Academic Editor: Muhammad Raziq Rahimi Kooh

In this study, Pb (II) removal from wastewater was investigated using a modified vitric crystal tuffite with a BET surface area of 11.7 m^2/g. For this purpose, tuffite was used in its natural and modified form with ethylenediaminetetraacetic acid (EDTA). Batch adsorption experiment was performed. The effects of contact time (0–90 min), adsorbent dosage (1–10 g/L), initial concentration (10–200 mg/L), and pH (2–12) on the removal of Pb (II) were investigated. The isotherm data were fitted to Langmuir, Freundlich, Temkin, and Redlich-Peterson isotherm models. Kinetic models such as pseudo-first-order, pseudo-second-order, and intraparticle diffusion models were used. In order to optimize the adsorption system and investigate the kinetic behaviour of adsorption, nonlinear isotherm and kinetic models were used as well as linearized models. Error analyses were made in order to express the obtained results more accurately. pH 5 was the optimum value for adsorption. According to nonlinear isotherm model calculations, Bayburt stone (BS) and its modified form (MBS) had q_{max} values of 335 and 584 mg/g, respectively. The Freundlich model, with its high correlation coefficients of about 1.00, was found to be more suitable for the adsorption of Pb (II) to MBS. The pseudo-second-order kinetic model with mean R^2 and k_2 values of 0.997 and 0.0116 1/min, respectively, was found to be more appropriate. According to the regeneration studies, the maximum desorption efficiency was 97.8%. The thermodynamic equilibrium coefficients obtained at different temperatures and ΔG^o, ΔH^o, and ΔS^o values were observed as -21.4, 46.4, and 163 kJ/mol, respectively. These values indicate that the adsorption of Pb (II) on to MBS was endothermic and spontaneous process. BS and MBS were characterized by different instrumental analyses such as SEM, EDS, FTIR, and zeta potential measurements.

1. Introduction

Interest in scientific studies on heavy metals has been increasing in recent years due to the carcinogenic effects of these substances and their dramatic deterioration in aquatic environments. Most heavy metals have negative effects on human health, even at low concentrations. Plants require small amounts of heavy metals such as copper, zinc, nickel, boron, iron, and molybdenum [1]. However, some heavy metals such as lead, mercury, cadmium, and arsenic are just the opposite. These substances have been blacklisted by various international organizations as they cause soil and water pollution as a result of activities such as industrial and urban waste discharges and fertilization. [2–5].

Lead is frequently used in battery, paint, and metal coating manufacturing processes [6]. Lead toxicity is associated with exposure to lead in air or water and has harmful effects on hematopoietic, kidney, reproductive, and central nervous systems as well as enzyme inhibition. Among heavy metals mentioned above, lead is considered to be one of the metals with the highest toxicity in its ionic state. Therefore, when it accumulates in living tissues, it has the property of being fatal [7]. Acute toxicity risks of lead must be reduced at every stage of the life cycle [8]. Although the action level of EPA is

15 ppb, lead concentrations are well above this level in most of the water bodies on the planet [9, 10].

Types, forms, and concentrations of heavy metals in water and wastewater play a primary determinant role in the selection of treatment processes. [2]. In addition, this selection depends on the economic conditions and discharge standards determined by the state institutions as well as the wastewater characteristics such as pH, temperature, flow rate, and biological oxygen demand. There are many traditional and novel wastewater treatment methods for lead treatment in the literature such as chemical precipitation [11]; micro-, ultra-, and nanofiltration [12]; reverse osmosis [13]; autocatalytic electrocoagulation [14]; capacitive deionization [15]; complex-assisted filtration [16]; electrocoagulation with low voltage [17]; biological lead removal [18]; and adsorption [6, 19]. However, since these technologies generally have higher costs and lower removal efficiencies, they have a more limited application area than adsorption. Among the most heavy metal removal processes, adsorption is one of the promising one due to its high efficiency, simple operation, and low cost [20].

In recent years, there have been many articles in the literature using adsorbent with various properties. One of the most critical points in adsorption studies is to prepare adsorbents with a large specific surface area and high adsorption efficiency as economical as possible. For example, although activated carbon is a very good adsorbent with other properties, it is considered an adsorbent with limited use due to its high cost and slow diffusion properties [5]. For this reason, adsorption studies have focused on reducing the cost and increasing the adsorption efficiency by modifying the adsorbents by chemical or physical methods in recent years [5, 21–23]. Improving the adsorption capacity by modifying the sorbent surface with chemical methods is a common and easier method than physical modification. In addition, it was stated that the selectivity of the adsorbent on metal ions after chemical modification increased more than other methods [24]. Ethylenediaminetetraacetic acid (EDTA) for the chemical modification of the adsorbent is one of the effective agents in metal adsorption since it forms strong metal complexes by chelating with metal ions through the complex formation mechanism [25]. For this reason, it has a widespread use in metal adsorption studies.

Bayburt stone (BS) is a natural vitric crystal tuffite that is abundant and quite cheap especially in the Eastern Anatolia Region of Turkey. In addition, there are very limited articles made with similar materials in the literature, but no adsorption studies have been found with this natural stone. It is thought that the study will yield useful results for natural materials with similar properties and also for the modification of natural stones to be used in adsorption.

The aim of this study is to investigate the usability of BS for Pb (II) adsorption and to reveal how its modified form (MBS) using EDTA changes the adsorption performance. In this way, it is thought that an effective and novel metal ion adsorbent will be presented to the field of application. In order to achieve this aim, the effects of operation parameters on adsorption, such as pH, temperature, mixing speed, time, adsorbate, and adsorbent concentrations, were investigated. In addition, behaviour of adsorption was tried to be revealed by analysing the kinetic models. All trials were performed for both raw and modified tuffite.

2. Materials and Methods

2.1. Chemicals. Aqueous $Pb(NO_3)^2$ stock solution at a concentration of 1000 mg/L Pb (II) was used in all experimental runs. HCl and NaOH, Na_2EDTA, and HNO_3 solutions were used for pH adjustments, for modifying the adsorbent, and for regenerating the adsorbent in desorption process, respectively. All the chemicals were of analytical reagent grade from E. Merck, Darmstadt, Germany.

2.2. Adsorbent. BS was obtained from Bayburt province in the Eastern Anatolia Region of Turkey. This material is an abundant and easily found regional stone within the borders of Bayburt province. The proved reserve of this stone in the region is 2,500,000 tons. BS has a unit weight of 2.38 g/cm^3 and a porosity of 23% [26]. As can be seen from Table 1, this tuffite has a lighter structure than most natural stones. It is thought that this feature of the adsorbent will provide an additional advantage in terms of operation in industrial adsorption applications.

Chemical components of BS are given in Table 2.

In the modification process of BS, the adsorbent samples were first cleaned with compressed air and washed several times with tap water. It was then passed through distilled water and allowed to dry for 24 hours in an oven at 105°C. The dried samples were ground and sieved to a grain size of 0.1 mm and below. Then, 100 g of the cleaned and dried stone samples was mixed with 1000 mL of 0.1 M NaOH and shaken for at least 3 hours. The mixture was filtered and the samples were cleaned with pure water until the pH value of the filtrate was approximately neutral. It was then left to dry in a drying oven at 105°C for at least 2 hours. The same procedures were repeated using EDTA to improve the selectivity of BS toward the adsorption of Pb (II). Prepared MBS and BS samples were stored in a moisture-free environment during the study.

2.3. Analyses. All analyses performed throughout the study were repeated at least three times. The results presented are given as the average of these trials. In addition, error function analyses were used to reveal the accuracy of the results.

pH measurements were made with CrisonpH25$^+$ brand pH meter device. All of the samples were centrifuged before Pb (II) analyses (Nüve NF 1200R). During the adsorption/desorption experiments, Pb (II) concentrations in the samples were measured at 283.3 nm wavelength, 10 mA current, and 0.5 nm slit width using Shimadzu AA6800 atomic adsorption spectrophotometer.

Scanning electron microscopy (SEM-EDS), Fourier-transform infrared spectroscopy (FTIR), and Brunauer-Emmett-Teller (BET) analyses were performed with ZEISS SIGMA 300, Bruker VERTEX 70v and Micromeritics 3 Flex instruments, respectively. These analyses were carried out in

Table 1: Average specific gravity of various stone types.

Name	Specific gravity (g/cm^3)
Andesite	2.22
Bayburt stone	2.38 (this study)
Rhyolite	2.4
Sandstone	2.58
Granite	2.67
Limestone	2.69
Marble	2.73
Basalt	2.77
Slate	2.77
Gabbro	3.00
Gneiss	3.12

[27].

Table 2: Chemical components of BS used in this study.

Component	Weight (%)
MgO	0.200-0.880
SiO_2	65-71
CaO	1.03-5.19
Fe_2O_3	0.23-0.93
TiO_2	0.09-0.16
Al_2O_3	10.4-12.5
Na_2O	0.25-2.3
K_2O	1.57-7.33

[28].

the laboratories of Atatürk University Eastern Anatolia High Technology Application and Research Centre (DAYTAM).

2.4. Zeta Potential Measurements. Zeta potential measurements were carried out with Malvern Zetasizer Nano ZSP brand device between pH 2 and 12, and the maximum potential value was obtained as -29.8 mV at pH 10.

2.5. Experimental Procedures. Adsorption experiments were carried out by using stoppered glass Erlenmeyer flasks (250 mL). 1000 mg/L stock solution of lead was prepared by dissolving required amount of $Pb(NO_3)_2$ in deionized water. Various amounts of BS or MBS (1 to 10 g) and solutions diluted in the range of 10 to 200 mg Pb/L from the stock solution according to the experimental conditions were added to Erlenmeyer flasks for each experiment.

With the help of the CrisonpH25+ model multiparameter, the pH of the mixture was kept between 2 and 12 using HCl and NaOH solutions to determine the optimum pH value, and then, experiments were carried out at the determined optimum pH value.

Experiments were carried out at 25, 30, 35, and 40°C temperature conditions with the aid of a heat-adjustable Edmund Bühler Incubator HoodTH15 brand shaker at the optimized pH value.

Stirring speeds of 100, 200, and 300 rpm were applied in the study, and the trials were initially continued for up to 300 minutes. After determining the time for adsorption to reach equilibrium, the experiments were continued with this mixing speed.

Adsorbed Pb (II) amount onto per unit weight of adsorbent (mg/g) is calculated with the following equation [29]:

$$q_e = \frac{(C_{o-}C_e).V}{m}, \quad (1)$$

where C_o and C_t are the Pb (II) concentrations (mg/L) at time *0* and *t*, V is the volume of the Pb (II) solution (L), and m is the weight of material (g).

The isotherm study, in which the adsorption capacity was tried to be determined, was carried out at the optimum pH value, using different temperatures (25 to 40°C), initial lead (10 to 200 mg/L), and adsorbent (1 to 10 g/L) concentrations. In the kinetic study to determine the adsorption rate, 5 different initial lead concentrations of 10, 25, 50, 100, and 200 mg/L were used. In each experiment, the remaining lead concentration analyses were made in the samples taken from the solution at certain time intervals.

2.6. Desorption Experiments. In order for the materials used as adsorbent to be widely used, their renewability is an important factor in addition to their properties such as adsorption capacities and costs. BS and MBS were subjected to desorption process to investigate their reusability after adsorption process. For this purpose, the adsorbent was regenerated by using 0.1 M HNO_3 solution and distilled water under mechanical stirring at 200 rpm for 8 hours at room temperature (25°C), and the amount of lead transferred to the solutions was evaluated with sampling at time intervals. In order to reveal the pH effect, the pH range of the regeneration solution was changed between 2 and 12 as in the adsorption procedure in this study. Adsorption and desorption processes were considered as a whole process in this study, and this procedure was carried out for all samples immediately after the completion of the adsorption process.

3. Results and Discussion

3.1. The Effect of the Operational Parameters. In the study, ambient pH, adsorbent amount, ambient temperature, mixing speed, and initial concentration were chosen as operational parameters, and the effect of all these parameters on adsorption was revealed.

pH is considered to be one of the most important parameters controlling adsorption, especially in metal ion adsorption processes. The acidity of the solution has a significant influence on the chemical behaviour and functionality of the material surface through the formation of hydrolysis, precipitation, ion exchange, and stable complexing with elements. [30]. If the pH in Pb (II) solution is below 3.30, the dominant species in the solution is Pb (II) ions, and as the pH approaches the neutral value, $Pb(OH)_2$ begins to precipitate in the solution [31]. In addition, at low pH values, the adsorbent surface will become overloaded and will begin to

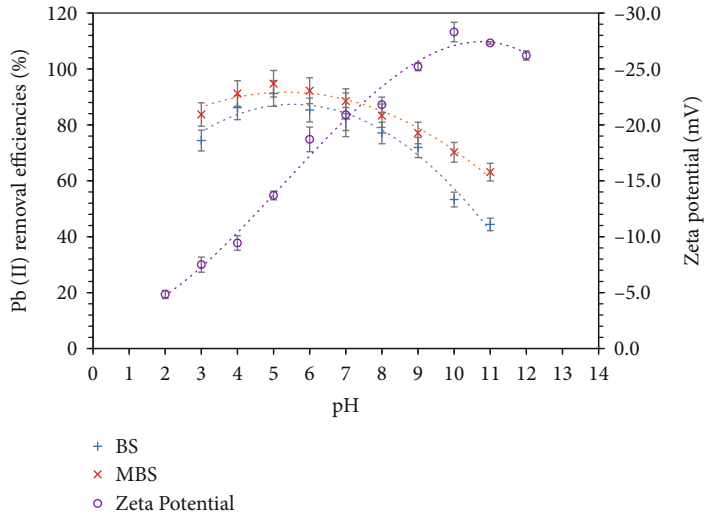

Figure 1: Zeta potentials and Pb (II) removal efficiencies versus pH for BS and MBS. ± SD shown by error bar.

remove metal ions from itself. Therefore, in both cases, the adsorption efficiencies are below the expected values [32]. For this reason, it is necessary to reveal the optimum pH value at which this balance is achieved in adsorption studies. In this research study, the experiments were carried out by keeping the pH between 2 and 12 in accordance with the literature, and first of all, the optimum pH value was investigated.

As seen in Figure 1, the maximum zeta potential value was actually obtained around pH 10. However, as mentioned above, Pb (II) removal efficiency was low as precipitation became dominant at this pH value. The maximum adsorption efficiencies obtained in the experiments were around pH 5, and at values above and below this value, the adsorption efficiencies decreased significantly due to precipitation and positive charging, respectively. In other words, lead ion adsorption increases due to electrostatic attraction between negatively charged adsorbent surface and positively charged cationic lead at this pH value. Figure 1 shows the relationship between pH and adsorption efficiency at 10 g/L adsorbent, 10 mg/L initial Pb (II) concentration, and 35°C conditions. The same behaviour of removal efficiency against solution pH was observed in all other conditions. Therefore, the optimum pH value for this study was accepted as 5, and effects of contact time, adsorbent concentration, mixing speed, and temperature on the Pb (II) adsorption ability of BS and MBS were investigated by adjusting the solution pH value to 5. Each trial was performed in at least three repetitions.

Figure 1 also shows the adsorption efficiency differences between BS and MBS. As seen in the figure, while the highest efficiency achieved with BS was 90%, this value increased to 95% and above with MBS. As can be seen, the adsorbent modification process increases the adsorption efficiency at all pH values.

To evaluate the effect of initial Pb (II) concentration on the adsorption, lead concentrations were applied in the range between 10 and 200 mg/L. The behaviour of the adsorption system for MBS with increasing lead concentrations is given in Figure 2(a). As can be seen in Figure 2(a), lead adsorption is highly influenced by the initial lead concentration. The amount of Pb (II) remaining in the solution increased with increasing initial concentration. Maximum adsorption efficiencies were found as 91.2% and 94.9% for BS and MBS, respectively, at 10 mg Pb (II)/L, 10 g adsorbent/L, 200 rpm, and 35°C conditions. These values were observed as 87.4% and 90.2% for BS and MBS, respectively, for initial Pb (II) concentration of 200 mg Pb (II)/L and under the same other conditions. As can be understood from these results, MBS showed higher capacity than BS in terms of adsorption efficiency. Experimental data revealed the same trend in other trials.

Figure 2(b) shows the change in the Pb (II) concentration remaining in the solution when the adsorbent dosage is changed from 1 mg/L to 10 mg/L. In this series of studies, the initial Pb (II) concentration, temperature, pH, and stirring speed were 10 mg/L at 35°C, 5, and 200 rpm, respectively. As can be seen in Figure 2(b), the concentration of Pb (II) remaining in the solution decreases as the adsorbent dosage increases from 1 to 10 g/L due to the presence of more adsorbent surface area in the solution. According to the data obtained, it is observed that the amount of Pb (II) adsorption increases rapidly up to the adsorbent dosage of 5 g/L, and the acceleration is slightly decreased up to 10 g/L, but there is still a significant increase. Since it was seen that the adsorption efficiency would not increase significantly in the adsorbent dosage increases after this point, the maximum adsorbent dosage was accepted as 10 g/L. Experiments showed that the system reached equilibrium in 90 minutes, and after this period, 0.68, 0.60, 0.53, and 0.51 mg/L Pb (II) concentrations remained in the solution at 1, 2, 5, and 10 g/L adsorbent dosages, respectively.

The effect of agitation speed on adsorption efficiency was investigated by changing the speed between 100 and 300 rpm (increasing 50 rpm in each trial). The agitation speed has an important role in adsorption processes. As can be seen from Figure 2(c), the amounts of adsorbed Pb (II) were increased with increasing speed until 200 rpm.

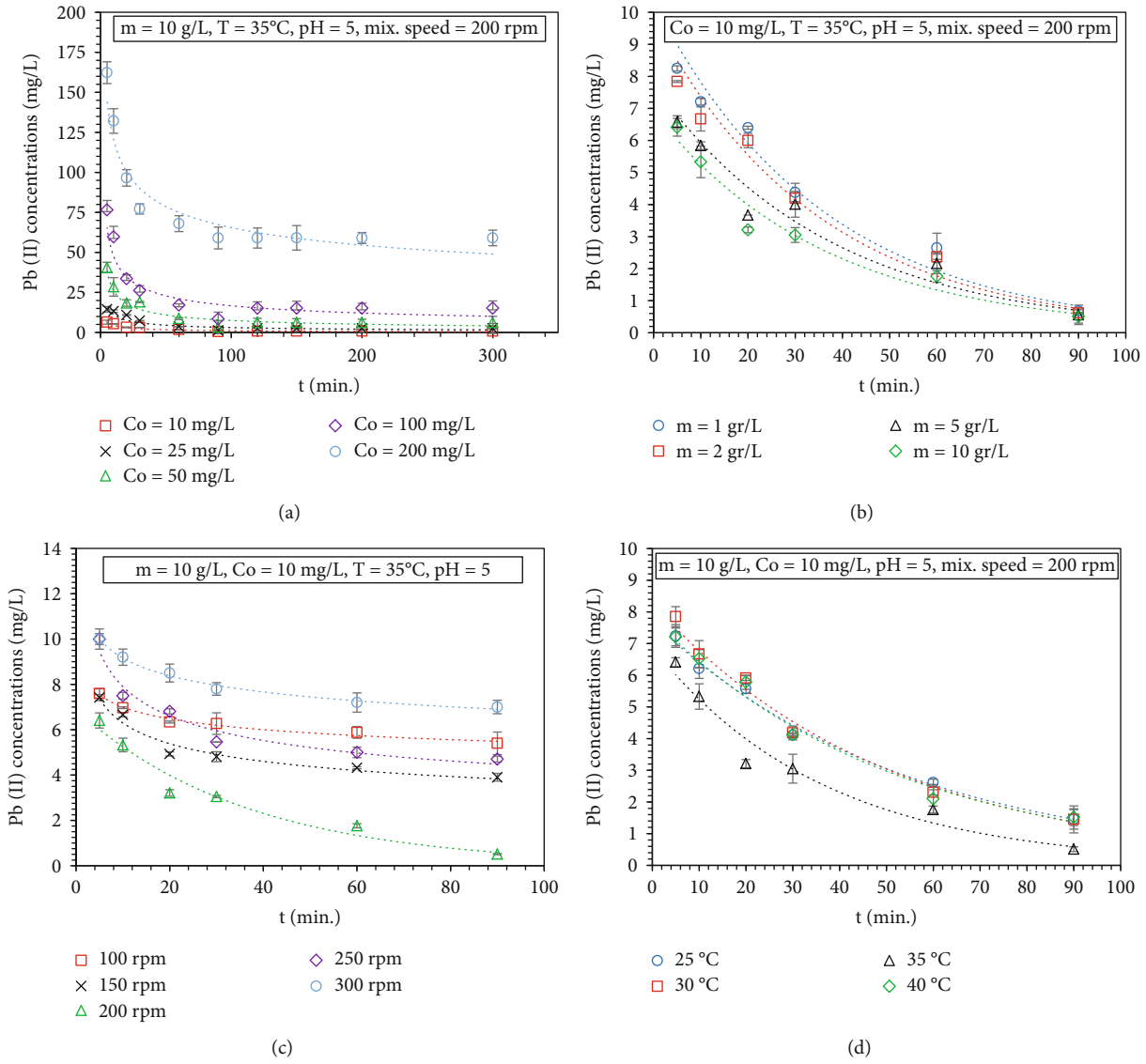

Figure 2: Pb (II) concentration changes over time at different conditions for MBS. ± SD shown by error bar.

The amount of Pb (II) removed at 250 rpm decreased slightly and reached the lowest level at 300 rpm. It is thought that this situation occurs because high mixing speeds cause a decrease in the boundary layer and decrease the bed resistance, resulting in a decrease in the amount of adsorbed material [33].

Temperature has a significant effect on increasing or decreasing the amount of adsorption. In this study, experiments to reveal the effect of temperature on adsorption were carried out at four different temperatures ranging from 25 to 40°C. Other conditions in these experiments were adjusted as 10 g/L adsorbent dose, 10 mg/L initial Pb (II) concentration, and pH 5. Figure 2(d) shows the variation of the amount of lead remaining in the solution with time. It was observed that temperature increases from 25 to 35°C affect the adsorption efficiency positively. The efficiencies tended to decrease with the increase in temperature from 35 to 40°C. This is due to the exothermic nature of the process or the decrease in the effect of physical forces at high temperature [34]. According to these results, it was seen that the best temperature value for Pb (II) adsorption with BS and MBS was 35°C.

As a result of these experiments, best values of contact time, adsorbent dosage, mixing speed, and temperature were observed as 90 min, 10 g/L, 200 rpm, and 35°C, respectively.

3.2. Characterization. Scanning electron microscopy (SEM-EDS), Fourier-transform infrared spectroscopy (FTIR), and Brunauer-Emmett-Teller (BET) analyses were performed to examine the characteristic structure of MBS. The BET and Langmuir surface area of MBS were 11.7 m^2/g and 55.6 m^2/g, respectively. Table 3 shows the specific BET surface area, $q_{max,}$ and BETr (BET surface area ratio) values of some modified adsorbents used in lead adsorption. BETr values represents the ratio of q_{max} to the BET surface area.

SEM imaging and EDS methods were used to examine the structure of MBS and to reveal the changes that may occur after adsorption. SEM analysis is a frequently used

Table 3: Surface area and q_{max} values of some modified adsorbents found in the literature and MBS.

Adsorbent	BET surface area (m^2/g)	q_{max} (mg/g)	BETr (mg/m^2)	References
H_3PO_4-HC	29.7	312	10.51	[35]
$MnFe_2O_4$ magnetic nanoparticles	69.3	263	3.8	[36]
Biosilica	143	120	0.84	[37]
KCC-1	299	38.8	0.131	[38]
Magnetic chitosan/graphene oxide	74.4	112	1.51	[39]
Ni-doped bamboo charcoal	263	143	0.54	[40]
Bayburt stone (MBS)	11.7	584	27.62	This study

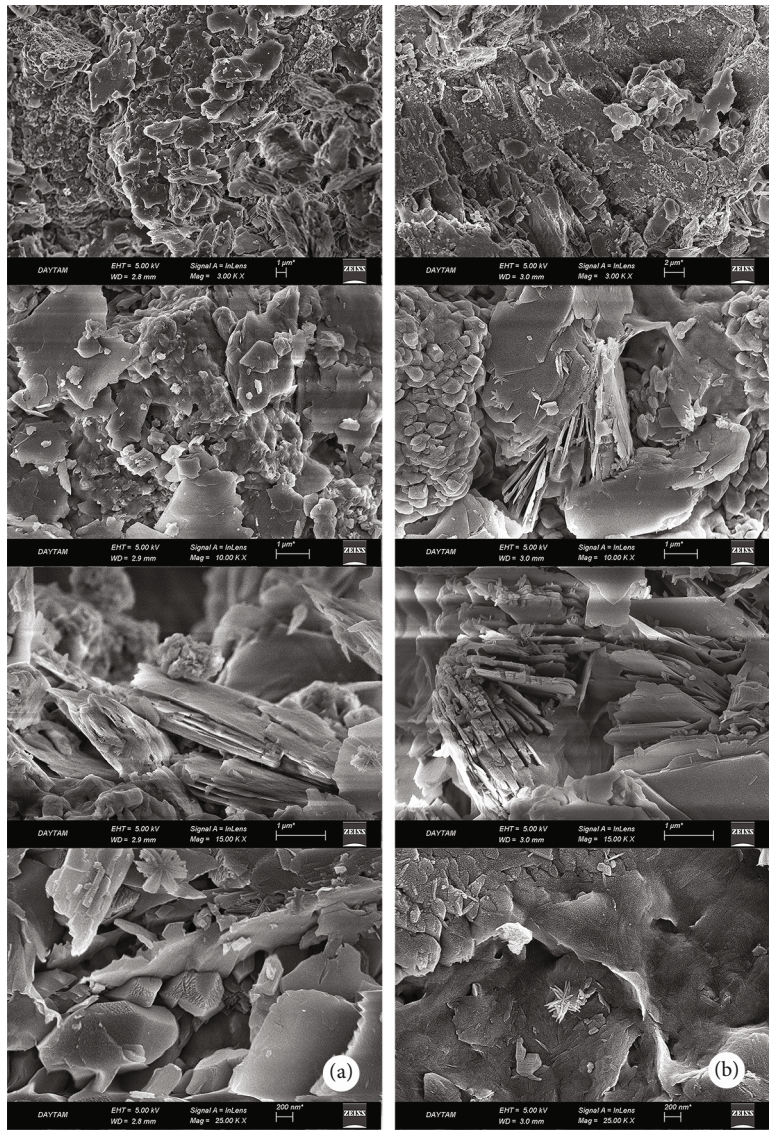

Figure 3: SEM images of MBS used in this study ((a) and (b) represent before and after adsorption, respectively).

method for surface morphology analysis of an adsorbent. SEM images of MBS before (Figure 3(a)) and after adsorption (Figure 3(b)) under optimum test conditions (pH = 5, $T = 35^{\circ}C$, $m = 10$ g/L, Co = 10 mg/L, and mixing speed = 200 rpm) are given in Figure 3. Surface and porous structure of MBS can be seen from both Figures 3(a) and 3(b). It can be seen from Figure 3 that the pores are quite heterogeneous and stack of the flake crystal structure with a sharp edge. When Figures 3(a) and 3(b) are compared, it is seen that although the morphology of this layered structure changes

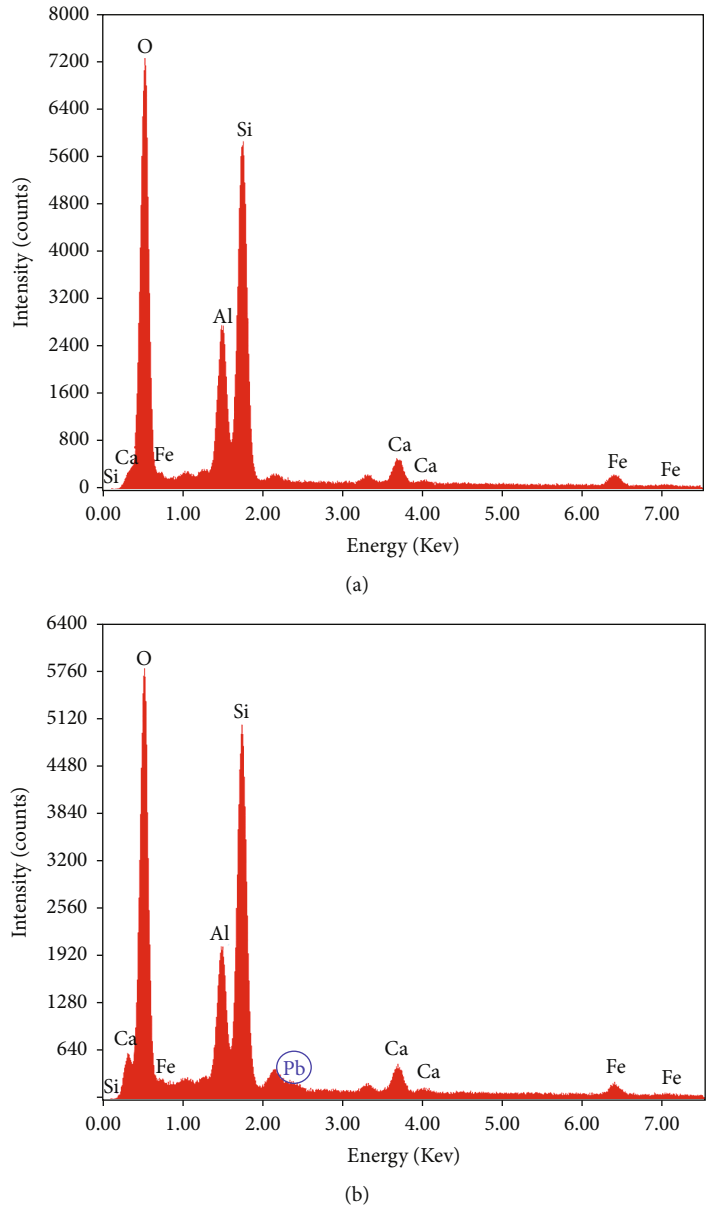

Figure 4: EDS graphs before (a) and after (b) Pb (II) adsorption.

slightly after adsorption, it still remains in a similar structure. It is thought that this heterogeneous porous structure of MBS has a positive effect on the adsorption efficiency.

The EDS graph is given in Figure 4. The components of the tuffite used in the study, which are given in Table 2, appeared significantly in the peaks in the EDS graph (Figure 4(a)). The lead peak, observed after adsorption, can be seen in EDS graphs of MBS (Figure 4(b)).

The surface chemistry characterisation of MBS was investigated by FTIR spectroscopy (Figure 5). As can be seen from Figure 5, FT-IR spectrum peaks of raw MBS have upper or lower transmittance values than those of after adsorption. Generally, FTIR spectra of the zeolitic tuff samples display a broad band at 3700–3100 cm^{-1} [41]. The broad, strong band around 3650 cm^{-1} can be assigned to the O–H stretching mode of hexagonal groups and adsorbed water [34]. The FTIR spectrum of MBS has asymmetric stretching vibrations (1025-1030 cm^{-1}) of Si–O–Al band [42]. Bands that appear in the region of 1025–980 cm^{-1} can be assigned to Si–O or Al-O stretching mode [43] and 536 cm^{-1} can be assigned to Si–O–Si(Al) bending [44].

3.3. Equilibrium Modelling

3.3.1. Langmuir Isotherm. Langmuir model equation is given in Equation (2) [45]:

$$q_e = \frac{q_{m K_L C_e}}{1 + K_L C_e}, \quad (2)$$

where q_m is the maximum adsorbate uptake capacity (mg/g) and K_L is the Langmuir constant related to the energy of

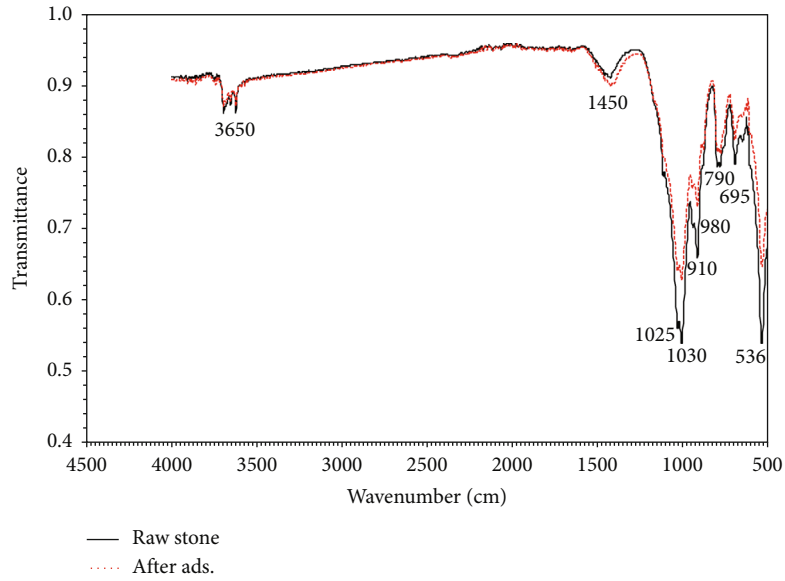

FIGURE 5: FTIR spectrum of Bayburt stone before and after Pb (II) adsorption.

adsorption (L/mg). Besides, the essential property of the Langmuir isotherm can be expressed in terms of the dimensionless constant separation factor R_L and values between 0 $< R_L <$ represent a favourable adsorption [23].

$$R_L = \frac{1}{1 + K_L C_o}. \quad (3)$$

3.3.2. Freundlich Isotherm. Freundlich model equation is given in Equation (4) [45].

$$q_e = K_F C_e^{1/n}, \quad (4)$$

where K_F is Freundlich constant related to biosorption capacity (L/g) and $1/n$ is the heterogeneity factor.

3.3.3. Temkin Isotherm. Temkin isotherm equation is given in Equation (5) [46].

$$q_e = BlnAC_e, \quad (5)$$

where $B = RT/b$, b is the Temkin constant related to heat of sorption (J/mol), A is the Temkin isotherm constant (L/g), R is the gas constant (8.314 J/mol.K), and T is the absolute temperature (K) of solution.

3.3.4. Redlich-Peterson Isotherm. Redlich-Peterson isotherm is given with Equation (6) [47].

$$q_e = \frac{AC_e}{1 + BC_e^{\,n}}, \quad (6)$$

where A (L/g) and B (mg/L) are Redlich-Peterson constants and n is the model exponent. The value of n is between 0 and 1. When this value approaches 0, the model behaves as the Freundlich isotherm, and when it approaches 1, it behaves as the Langmuir isotherm [47].

The batch equilibrium technique was used to examine the adsorption isotherms of Pb (II) on BS and MBS. Experiments were carried out in a temperature-controlled shaker. Different temperature (25-45°C), different adsorbent dose (1-10 g/L), and different initial lead concentration (10-200 mg/L) ranges were applied for modelling. The remaining Pb (II) concentrations in the solution were analysed in the samples taken at various time intervals. The results from the isotherm study were used to evaluate the applicability of the Langmuir, Freundlich, Temkin, and Redlich-Peterson isotherm models. Figure 6 shows the linear model plots of these isotherms.

In order to obtain more realistic isotherm factors and parameters in isotherm modelling calculations, nonlinear isotherm calculations have been made as well as linear ones. Nonlinear and linear isotherm model constants are given in Table 4 for different operating conditions. In addition, the error analyses presented in Table 5 were also used to more accurately assess the fit of the isotherm models to the experimental data. [48]. All calculations are carried out using OriginPro 2022b.

It can be seen from Table 4 that the R^2 correlation coefficients of the models in the nonlinear approach are higher than the linear ones. Although this study shows that the linearization technique can help in determining the optimum sorption isotherm, it is noteworthy that the Redlich Peterson isotherm, which has the lowest R^2 levels in the linear approach, has quite good correlation coefficients in the nonlinear approach. Although not in the same amount, some improvement in R^2 values is also observed in Langmuir and Freundlich isotherms. This situation revealed that the linear approach to reveal the optimum isotherm may not always give accurate results [49]. On the other hand, R^2 values obtained for MBS were always higher than BS for

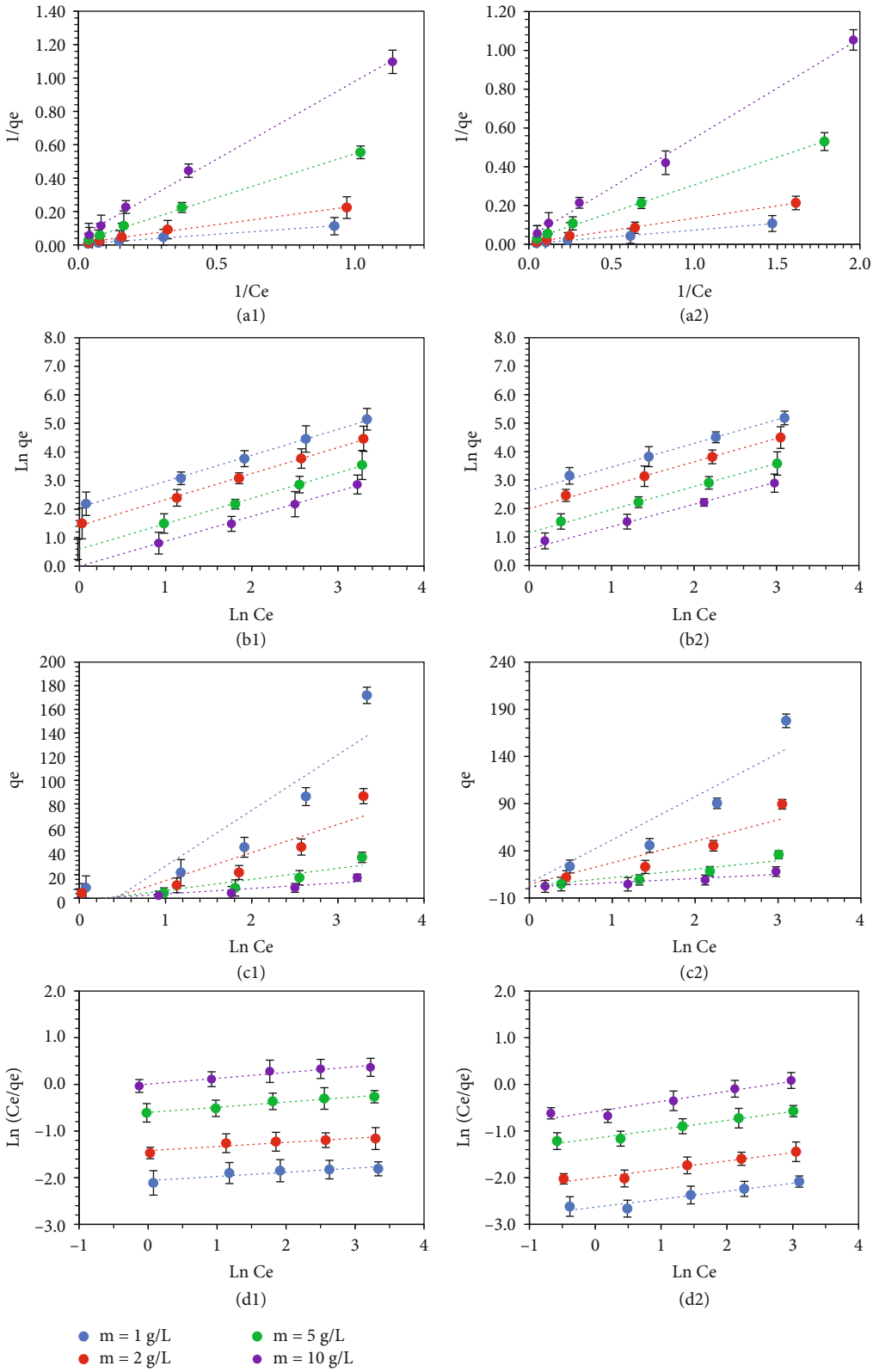

Figure 6: Langmuir, Freundlich, Temkin, and Redlich-Peterson isotherm model plots with linear estimation at 35°C, pH 5, and 200 rpm operating conditions for BS (a1, b1, c1, and d1, respectively) and MBS (a2, b2, c2, and d2, respectively). ± SD shown by error bar.

Table 4: Isotherm model parameters of Pb (II) adsorption for various temperatures.

Model	BS			MBS		
	25°C	30°C	35°C	25°C	30°C	35°C
Linear						
Langmuir						
q_m (mg/g)	107	161	215	229	288	322
K_L (L/mg)	0.045	0.028	0.040	0.020	0.017	0.044
R^2	0.991	0.998	0.995	0.999	0.999	0.997
Freundlich						
K_F (L/g)	5.01	4.97	7.87	4.82	5.07	13.9
$1/n$	0.771	0.813	0.911	0.881	0.888	0.829
R^2	0.999	0.999	0.998	0.999	0.999	0.996
Temkin						
A (L/g)	0.408	0.407	0.657	0.410	0.429	1.140
b (J/mol)	75.6	72.3	55.2	63.4	61.7	56.9
R^2	0.836	0.858	0.823	0.841	0.849	0.867
Redlich-Peterson						
A (L/g)	1.19	2.07	3.82	1.57	2.46	4.66
B (mg/L)	0.153	0.220	0.214	0.173	0.221	0.323
n	0.256	0.316	0.326	0.275	0.32	0.188
R^2	0.811	0.759	0.763	0.818	0.837	0.886
Nonlinear						
Langmuir						
q_m (mg/g)	231	286	335	336	418	584
K_L (L/mg)	0.024	0.019	0.043	0.011	0.019	0.022
R^2	0.993	0.998	0.997	0.999	0.999	0.998
Freundlich						
K_F (L/g)	4.82	5.07	13.9	4.94	5.31	13.6
$1/n$	0.881	0.888	0.829	0.885	0.896	0.831
R^2	0.999	0.999	0.999	0.999	0.998	0.999
Redlich-Peterson						
A (L/g)	1.22	2.17	4.22	1.68	3.62	5.22
B (mg/L)	0.157	0.235	0.332	0.193	0.348	0.412
n	0.763	0.746	0.686	0.875	0.852	0.918
R^2	0.983	0.989	0.988	0.997	0.996	0.997

the trials performed under the same conditions. Error analyses also confirm this situation due to smaller error values (Table 5). These results suggest that the applied modification process will make the adsorbent more useful. As can be clearly seen from Table 4, the Temkin isotherm model is the least suitable model for the adsorption of lead on BS or MBS among the other models examined in this study. Correlation coefficients of this isotherm have the smallest values obtained in the study (average 0.839 for BS and 0.852 for MBS). According to the nonlinear approach, R^2 values of Langmuir, Freundlich, and Redlich Peterson isotherms were obtained as 0.997, 0.999, and 0.988 for BS and 0.998, 0.999, and 0.997 for MBS, respectively. Therefore, it can be said that Langmuir, Freundlich, and Redlich Peterson models are suitable for the adsorption of Pb (II) on BS and MBS. However, it would not be wrong to say that adsorption is multilayered and reversible because R^2 values of Freundlich model are slightly higher than that of Langmuir and Redlich Peterson in most cases. This result can also be seen in Figure 7. When the Ce versus qe plot is examined, it is seen that the best fit to the isotherm curve is obtained with Freundlich nonlinear curve. According to the nonlinear calculations, Langmuir maximum adsorption capacity of BS and MBS was observed at 35°C as 335 and 584 mg/g, respectively (Table 4). Although the Bayburt stone has a smaller BET surface area than most adsorbents, this q_m values are quite high and usable for real applications (Table 3). It is one of the most important findings of this study. On the other

Table 5: Error analysis of isotherm adsorption parameters.

Model	BS			MBS		
	25°C	30°C	35°C	25°C	30°C	35°C
Langmuir						
ARE	15.7	15.1	14.5	12.8	8.74	8.30
SSE	0.031	0.041	0.037	0.025	0.023	0.031
X^2	0.221	0.169	0.137	0.234	0.109	0.158
R^2	0.993	0.998	0.997	0.999	0.998	0.999
Adj. R^2	0.992	0.997	0.996	0.997	0.998	0.998
Freundlich						
ARE	6.72	7.13	8.18	5.16	7.22	4.19
SSE	0.203	0.266	0.217	0.178	0.113	0.091
X^2	0.342	0.361	0.287	0.217	0.193	0.211
R^2	0.999	0.999	0.999	0.999	0.998	0.999
Adj. R^2	0.998	0.998	0.999	0.998	0.998	0.998
Redlich-Peterson						
ARE	3.22	4.22	3.83	3.17	3.54	3.63
SSE	0.093	0.075	0.071	0.054	0.058	0.043
X^2	0.341	0.234	0.196	0.134	0.083	0.064
R^2	0.983	0.989	0.988	0.997	0.996	0.997
Adj. R^2	0.992	0.988	0.988	0.996	0.995	0.997

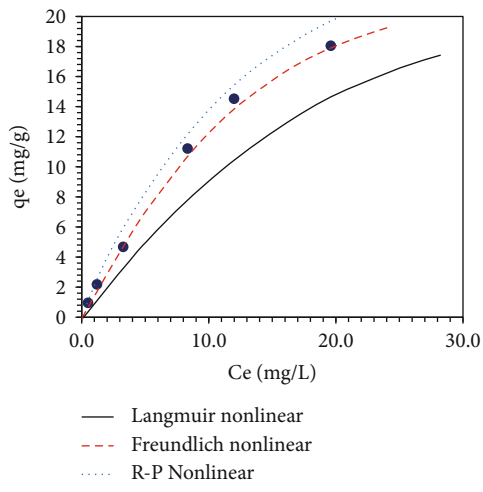

Figure 7: Adsorption isotherm for Pb (II) on MBS ($T = 35$°C, $m = 10$ g/L).

hand, it can be said that the Pb (II) adsorption on Bayburt stone is favourable since K_L values of Langmuir and $1/n$ values of Freundlich were smaller than 1 for all operating conditions [50]. For all conditions in this study, the calculated dimensionless constant R_L was between 0 and 1. This reveals that adsorption is the favourable [23].

3.4. Adsorption Kinetics. In order to reveal the reaction rate, pseudo-first-order, pseudo-second-order kinetic models, and intraparticle kinetic model representing diffusional

Table 6: Kinetic model parameters of Pb (II) adsorption at 35°C.

C_o (mg/L)	10	25	50	100	200
qe_{exp} (mg/g)	9.32	23.4	45.7	90.4	178
Linear					
Pseudo-first order					
qe_{cal} (mg/g)	8.95	19.3	40.5	87.4	168
k_1 (1/min)	0.025	0.024	0.029	0.032	0.026
R^2	0.966	0.986	0.872	0.993	0.969
Pseudo-second order					
qe_{cal} (mg/g)	10.4	25.0	48.4	93.8	174
k_2 (1/min)	0.017	0.013	0.011	0.016	0.017
R^2	0.976	0.996	0.981	0.992	0.993
Intraparticle diffusion					
Kp (mg/g.min$^{0.5}$)	0.126	0.221	0.168	0.114	0.165
C (mg/g)	4.24	11.6	29.3	63.3	122
R^2	0.977	0.984	0.924	0.962	0.979
Nonlinear					
Pseudo-first order					
qe_{cal} (mg/L)	9.02	21.2	47.4	91.8	177
k_1 (1/min)	0.018	0.018	0.019	0.012	0.017
R^2	0.975	0.991	0.982	0.994	0.981
Pseudo-second order					
qe_{cal} (mg/L)	9.53	24.7	52.2	96.2	178
k_2 (1/min)	0.011	0.012	0.009	0.017	0.009
R^2	0.992	0.997	0.996	0.997	0.998
Intraparticle diffusion					
Kp (mg/g.min$^{0.5}$)	0.121	0.106	0.092	0.077	0.059
C (mg/g)	7.25	23.6	63.2	83.2	191
R^2	0.981	0.985	0.941	0.972	0.981

kinetics were used. And to make the results more useful, these models were analysed in both linear and nonlinear forms. Equations of these models are given in [39, 51]

$$q_t = q_e[1 - \exp(k_1 t)], \tag{7}$$

$$q_t = \frac{q_e^2 k_2 t}{1 + (k_2 q_e t)}, \tag{8}$$

$$q_t = K_p t^{0.5} + C, \tag{9}$$

where k_1 (1/min) and k_2 (g/mg.min) are the adsorption rate constants of first-order and second-order kinetic models, respectively, q_e (mg/g) is the equilibrium adsorption uptake and q_t (mg/g) is the adsorption uptake at time t (min), Kp (mg/g.min$^{0.5}$) is the initial rate of intraparticle diffusion, and C (mg/g) is the intercept related to the thickness of the boundary layer. Results of kinetic study are given in Table 6 for MBS at 35°C. Figures 8(a)–8(c) show the linearised pseudo-first-order, pseudo-second-order, and intraparticle kinetic model plots, respectively, at 35°C, pH 5, and 200 rpm operating conditions for MBS. Nonlinear

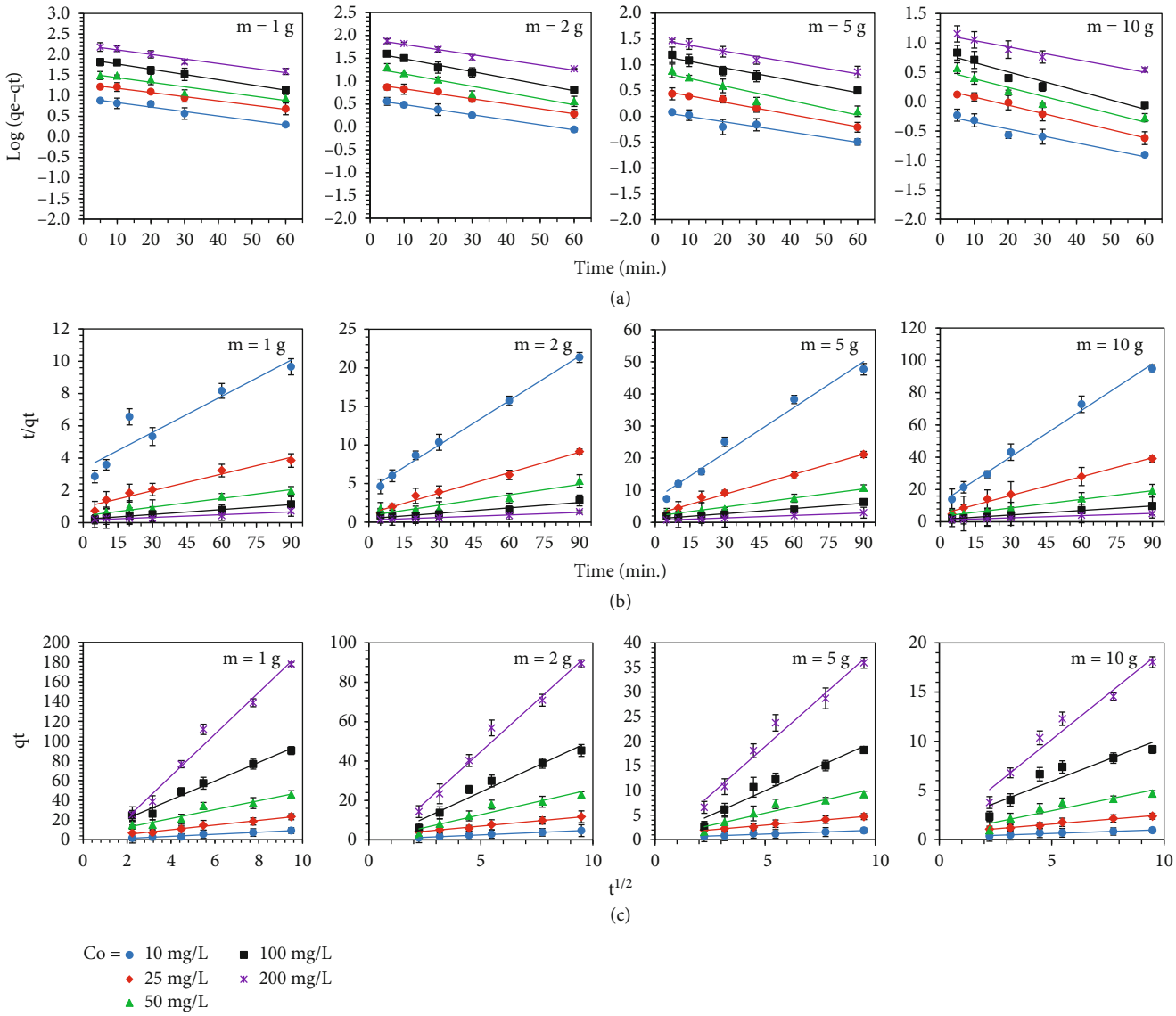

FIGURE 8: Pseudo-first-order (a), pseudo-second-order (b), and intraparticle (c) kinetic model plots at 35°C, pH 5, and 200 rpm operating conditions for MBS. ± SD shown by error bar.

kinetic model curves can be seen in Figure 9. Error analyses of kinetic adsorption parameters are given in Table 7.

Five different concentrations were used in the study, with an initial concentration of Pb (II) in the range of 10 to 200 mg/L. When the results given in Table 6 are evaluated, it is seen that the pseudo-second-order kinetic model has more appropriate values than the other models studied. In this study, the order of magnitude of the correlation coefficients is pseudo-second-order > intraparticle diffusion > pseudo-first-order. The values of qe_{cal} (calculated from the model) were closer to the values of qe_{exp} (experimentally measured) in pseudo-second-order model. According to these correlation coefficients and error analyses given in Table 7, it is understood that the most suitable model for the adsorption of Pb (II) on MBS is the pseudo-second-order kinetic model, which indicates that the adsorption is controlled by chemical adsorption. The pseudo-first-order kinetic model assumes that the rate of adsorption is controlled by liquid membrane diffusion, while the pseudo-second-order kinetic model assumes that the rate is controlled by chemical adsorption. In addition, thanks to the intraparticle diffusion model, it can be understood whether the rate limiting step of the adsorption rate is intraparticle diffusion. In addition, the smaller the adsorption rate constants (k), the stronger the affinity of the adsorbent region, so the adsorption process is faster and more convenient [52]. The smallest rate constants obtained in this study belong to the pseudo-second-order kinetic model (0.0116 on average). In addition, it is seen that the k values obtained in the study using MBS are smaller than those of BS under the same conditions. For example, the k_2 values obtained in the study performed at 35°C temperature and 10 g/L MBS concentration were 0.017, 0.013, 0.011, 0.016, and 0.017 1/min for the initial concentrations of 10, 25, 50,

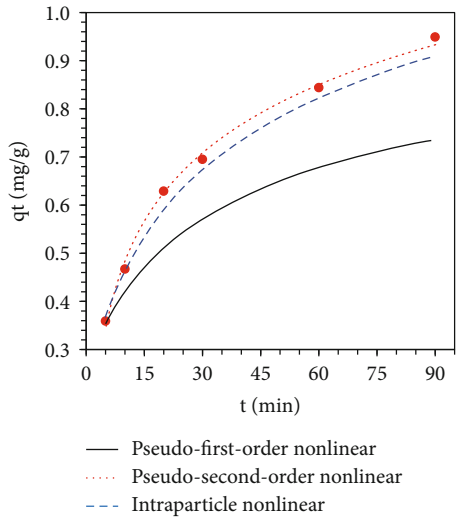

Figure 9: Sorption kinetics of Pb (II) onto MBS and nonlinear fits of pseudo-first-order, pseudo-second-order, and intraparticle diffusion models ($T = 35^{\circ}C$, $m = 10$ g/L).

Table 7: Error analysis of kinetic adsorption parameters.

C_o (mg/L)	10	25	50	200
Pseudo-first order				
ARE	48.3	44.1	32.7	46.6
SSE	0.628	0.575	1.132	0.594
X^2	2.31	2.09	3.16	1.93
R^2	0.975	0.991	0.982	0.981
Adj. R^2	0.974	0.990	0.981	0.981
Pseudo-second order				
ARE	6.25	6.01	4.14	6.10
SSE	0.114	0.105	0.093	0.081
X^2	0.384	0.218	0.344	0.193
R^2	0.992	0.997	0.996	0.998
Adj. R^2	0.991	0.996	0.995	0.997
Intraparticle diffusion				
ARE	18.27	15.68	13.22	17.30
SSE	0.321	0.265	0.354	0.198
X^2	1.247	1.632	1.192	1.037
R^2	0.981	0.985	0.941	0.981
Adj. R^2	0.980	0.984	0.940	0.980

100, and 200 mg/L Pb (II), respectively. However, in the study using BS, these values were calculated as 0.027, 0.024, 0.020, 0.025, and 0.024 1/min for the same conditions, respectively. These results show that MBS has better adsorbent performance than BS.

The comparison of the equilibrium adsorption uptake (qe) values obtained from the experimental results and calculated by the kinetic models is also important in terms of revealing which kinetic model is more suitable. The qe_{cal} values of the pseudo-second-order kinetic model were quite close to the qe_{exp} values (Table 6). A significant improvement in the values obtained in the nonlinear approach draws attention here as well. For example, while the qe_{cal} value obtained at the initial Pb (II) concentration of 10 mg/L was 10.4 mg/g in linear calculations, this value was found to be 9.53 mg/g, which is closer to the qe_{exp} value of 9.32 mg/g in nonlinear calculations. A similar situation was observed in pseudo-first-order kinetic and intraparticle diffusion models. However, as can be seen in Table 5 for the intraparticle model under the same conditions, the C value was slightly further away from the experimental data as 4.24 and 7.25 mg/g in linear and nonlinear calculations, respectively. According to these results, it can be said that the linear curve of the model does not pass through the origin and accordingly, and particle diffusion is not the only rate-limiting step in the adsorption of lead on BS or MBS. As a result, since the obtained results reveal that the pseudo-second-order model is more suitable to explain the kinetics of Pb (II) adsorption to BS and MBS, it can be said that the sorption is controlled by the chemisorption process [39, 53].

Table 8: Adsorption thermodynamic parameters of Pb (II) on BS and MBS at 100 mg/L of initial concentrations.

Temperature (°C)	ΔG^o (kj/mol)		ΔH^o (kj/mol)		ΔS^o (j/mol.K)	
	BS	MBS	BS	MBS	BS	MBS
25	-23.4	-17.7				
30	-23.9	-19.2	40.9	117	46.4	163
35	-25.1	-21.4				

3.5. Adsorption Thermodynamics. In addition to the isotherm and kinetic models, it is also useful to investigate the adsorption thermodynamics to define the affinity of the adsorbent for adsorption [33, 40, 54–56]. The thermodynamic parameters can be calculated using the following equations:

$$\Delta G^o = -RTlnK, \tag{10}$$

$$\Delta G^o = \Delta H^o - T\Delta S^o, s \tag{11}$$

where R is the universal gas constant (8.314 J/mol.K), T is the temperature (Kelvin), and K is the isotherm equilibrium constant (L/mol). ΔH^o and ΔS^o values then can be calculated from the intercept and slope of ΔG^o versus T plot (Equation (11)). In this research, ΔG^o values were calculated as -25.1 and -21.4 kJ/mol for BS and MBS, respectively at 35°C. This value of ΔG^o indicates that the adsorption process of lead on Bayburt stone is favourable and spontaneous. The ΔG^o values are negative at all temperatures but decreased slowly with increasing temperature [33]. In addition, the positive values of ΔH^o and ΔS^o indicate the process is endothermic in nature and increases randomly at the solid-solution interface [22]. These values were calculated as 40.9 and 117 kJ/mol for BS, respectively, and 46.4 and 163 kJ/mol for MBS, respectively. ΔG^o, ΔH^o, and ΔS^o values of the adsorption thermodynamics are given in Table 8.

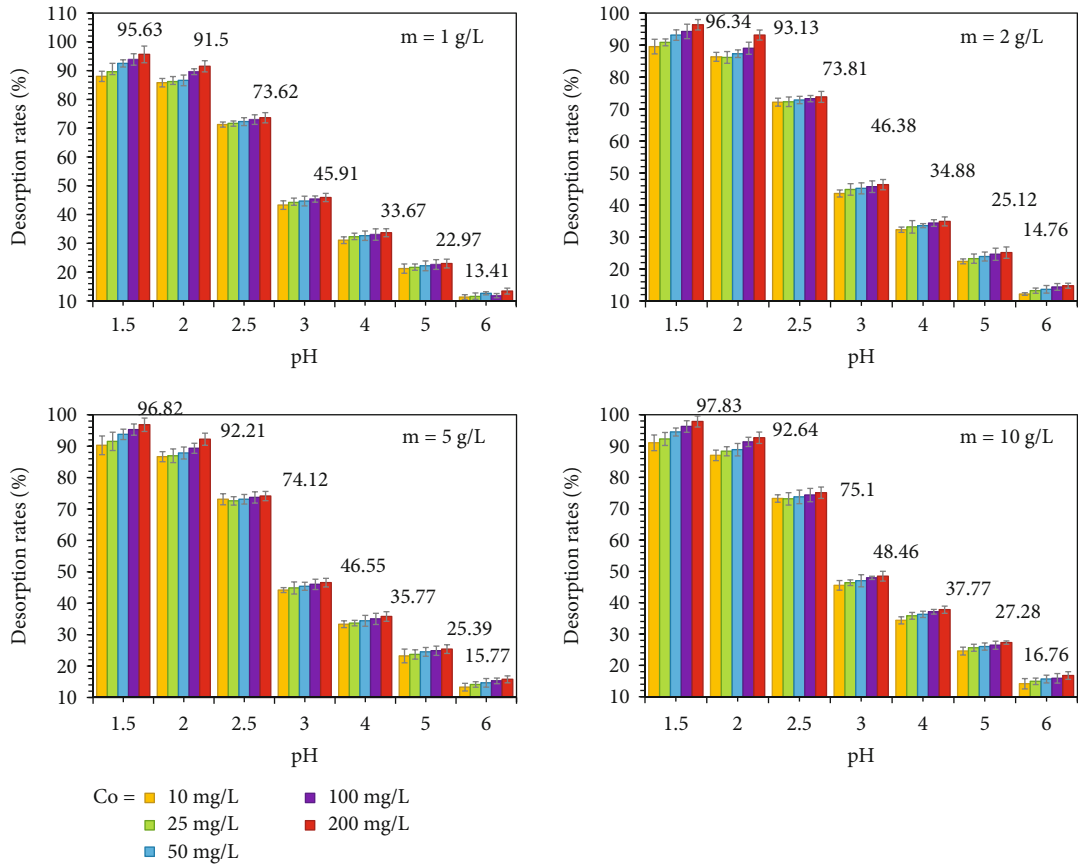

Figure 10: Desorption rates of Pb (II) versus pH graphs for different adsorbent dosages. ± SD shown by error bar.

3.6. Regeneration. Since pH is one of the most important parameters in desorption processes, desorption experiments were carried out at different solution pH values [57]. For this purpose, samples obtained from batch adsorption experiments, which were repeated enough for desorption experiments to be carried out at different pH values, were filtered through filter paper, rinsed with distilled water 3 times to eliminate free Pb (II) and placed in solutions brought to different acidic pH values using 0.1 M HNO_3. Samples were taken from the solutions at intervals of 5 to 10 minutes and Pb (II) analyses were performed. As a result of the analysis, the desorption ratio [52] of BS and MBS was calculated with the help of the following equation:

$$\text{Des.ratio} = \frac{VC}{mq_e} x\, 100\%, \tag{12}$$

where V is the volume of the desorption solution (L), C is the Pb (II) concentration in the desorption solution (mg/L), m is the amount of the adsorbent in the desorption experiment (g), and q_e is the amount of Pb (II) adsorbed onto the adsorbent in the adsorption (mg/g). Desorption rates versus pH graphs are given in Figure 10.

As can be clearly seen from Figure 10, the desorption of lead from MBS is highly related to the pH of the solution. In this study, while adsorption was maximum at pH 5, the maximum value of desorption was reached as 97.8% at pH 1 for 10 g/L sorbent concentration. As the ambient pH value increased, the desorption amounts decreased rapidly (16% at pH 6). In addition, desorption efficiencies increased with increasing adsorbent concentrations and initial Pb (II) concentrations. According to these results, it can be said that MBS has a very stable structure during the adsorption/desorption of Pb (II) and is a reusable sorbent for removal of Pb (II).

4. Conclusions

In summary, both BS and MBS are suitable for Pb (II) adsorption. Significant improvements were observed in the isotherm model correlation coefficients, q_{max} values, adsorption efficiencies, rate coefficients, and uptake values obtained with kinetic models, and even error analysis values with the modification process with EDTA.

The MBS exhibited excellent adsorption performance for Pb (II) with q_{max} of 584 mg/g. Maximum adsorption occurred at pH 5 and 35°C for 10 g/L adsorbent and 10 mg/L initial Pb (II) concentration. It was also confirmed that the adsorption process is pH dependent and the optimum pH for Pb (II) removal is 5.5. The adsorption was multilayered and reversible, as the Freundlich isotherm model correlated better than the Langmuir and Redlich-Peterson models for the adsorption of Pb (II) on MBS. The predominant process of adsorption of Pb (II) was attributed to chemical reactions compared to intraparticle or liquid membrane

diffusion, as the kinetic data gave more favourable values for pseudo-second-order kinetics. The thermodynamic study also reveals that the adsorption efficiency is more favourable at 35°C than 25°C. Since adsorbed Pb (II) can be desorbed with an efficiency of over 97%, MBS has been shown to be quite stable and reusable. In addition, this regional stone, which is used as an adsorbent in the study, is a completely natural material and has been modified with a simple method. Although the stone used in this study is a regional stone, it can be said that it will have a widespread use because there are many stones with similar properties around the world. Easy availability, low price, and high performance, which are important features of the materials used in adsorption studies, were obtained with this natural stone. The most important limiting factor in the use of this material as an adsorbent is its relatively low surface area. Although this situation did not affect the adsorption efficiency much in this study, attempts to increase the surface area may provide higher heavy metal adsorption efficiencies. However, further studies should be conducted with different types of heavy metals separately or in combination with a few heavy metals in order to make the use of MBS for heavy metal adsorption especially in industrial applications.

Data Availability

The data used to support the findings of this study are included within the article.

Conflicts of Interest

The authors declare that there are no conflicts of interest regarding the publication of this paper.

Acknowledgments

This research was carried out in Atatürk University Engineering Faculty Environmental Engineering Department research laboratories. The authors would like to thank the staff of Ataturk University East Anatolia High Technology Application and Research Center (DAYTAM).

References

[1] K. H. Vardhan, P. S. Kumar, and R. C. Panda, "A review on heavy metal pollution, toxicity and remedial measures: current trends and future perspectives," *Journal of Molecular Liquids*, vol. 290, article 111197, 2019.

[2] P. Kumar and S. R. Gayathri, "Adsorptıon of Pb2+ ions from aqueous solutions onto Bael tree leaf powder: isotherms, kinetics and thermodynamics study," *Journal of Engineering Science and Technology*, vol. 4, no. 4, pp. 381–399, 2009.

[3] L. Liu, W. Li, W. Song, and M. Guo, "Remediation techniques for heavy metal-contaminated soils: principles and applicability," *Science of the total environment*, vol. 633, pp. 206–219, 2018.

[4] M. Edelstein and M. Ben-Hur, "Heavy metals and metalloids: Sources, risks and strategies to reduce their accumulation in horticultural crops," *Scientia Horticulturae*, vol. 234, pp. 431–444, 2018.

[5] X. Chen, G. Zhang, J. Li, and P. Ji, "Possibility of removing Pb and cd from polluted water by modified fly ash," *Adsorption Science & Technology*, vol. 2021, article 1336638, pp. 1–8, 2021.

[6] M. Basu, A. K. Guha, and L. Ray, "Adsorption of lead on cucumber peel," *Journal of Cleaner Production*, vol. 151, pp. 603–615, 2017.

[7] J. Cruz-Olivares, C. Pérez-Alonso, C. Barrera-Díaz, F. Ureña-Nuñez, M. C. Chaparro-Mercado, and B. Bilyeu, "Modeling of lead (II) biosorption by residue of allspice in a fixed-bed column," *Chemical Engineering Journal*, vol. 228, pp. 21–27, 2013.

[8] P. Billen, E. Leccisi, S. Dastidar et al., "Comparative evaluation of lead emissions and toxicity potential in the life cycle of lead halide perovskite photovoltaics," *Energy*, vol. 166, pp. 1089–1096, 2019.

[9] M. Ahmaruzzaman and V. K. Gupta, "Rice husk and its ash as low-cost adsorbents in water and wastewater treatment," *Industrial & Engineering Chemistry Research*, vol. 50, no. 24, pp. 13589–13613, 2011.

[10] M. J. Brown and S. Margolis, ""Lead in drinking water and human blood lead levels in the United States," US Department of Health and Human Services," *Centers for Disease Control and Prevention*, vol. 61, pp. 1–9, 2012.

[11] L. Wang, K. Y. Hung, and T. N. Shammas, *Handbook of Environmental Engineering: Physicochemical Treatment Processes*, The Humana Press Inc., Totowa, NJ, first edition edition, 2005.

[12] F. Fu and Q. Wang, "Removal of heavy metal ions from wastewaters: a review," *Journal of Environmental Management*, vol. 92, no. 3, pp. 407–418, 2011.

[13] R. C. A. Moura, D. A. Bertuol, C. A. Ferreira, and F. D. R. Amado, "Study of chromium removal by the electrodialysis of tannery and metal-finishing effluents," *International Journal of Chemical Engineering*, vol. 2012, Article ID 179312, 7 pages, 2012.

[14] F. Y. AlJaberi, "Studies of autocatalytic electrocoagulation reactor for lead removal from simulated wastewater," *Journal of Environmental Chemical Engineering*, vol. 6, no. 5, pp. 6069–6078, 2018.

[15] Q. Dong, X. Guo, X. Huang et al., "Selective removal of lead ions through capacitive deionization: role of ion-exchange membrane," *Chemical Engineering Journal*, vol. 361, pp. 1535–1542, 2019.

[16] Y. Manawi, G. McKay, N. Ismail, A. Kayvani Fard, V. Kochkodan, and M. A. Atieh, "Enhancing lead removal from water by complex-assisted filtration with acacia gum," *Chemical Engineering Journal*, vol. 352, pp. 828–836, 2018.

[17] X. Rao, Q. Li, C. Inoue et al., "Simultaneous removal of lead(II) and nitrate from water at low voltage," *Journal of Water Process Engineering*, vol. 32, p. 100940, 2019.

[18] K. Zhang, Y. Xue, H. Xu, and Y. Yao, "Lead removal by phosphate solubilizing bacteria isolated from soil through biomineralization," *Chemosphere*, vol. 224, pp. 272–279, 2019.

[19] R. Bardestani, C. Roy, and S. Kaliaguine, "The effect of biochar mild air oxidation on the optimization of lead(II) adsorption from wastewater," *Journal of Environmental Management*, vol. 240, pp. 404–420, 2019.

[20] Q.-X. Liu, Y.-R. Zhou, M. Wang et al., "Adsorption of methylene blue from aqueous solution onto viscose-based activated carbon fiber felts: kinetics and equilibrium studies," *Adsorption Science & Technology*, vol. 37, no. 3-4, pp. 312–332, 2019.

[21] Y. Li, L. Peng, and W. Li, "Adsorption behaviors on trace Pb2+ from water of biochar adsorbents from konjac starch," *Adsorption Science & Technology*, vol. 38, no. 9-10, pp. 344–356, 2020.

[22] J. Ren, L. Zheng, F. Yang et al., "Electron-scale insights into the single and coadsorption Cd(II) behaviors of a metal-nonmetal-modified titanium dioxide," *Adsorption Science & Technology*, vol. 2021, article 4556493, pp. 1–15, 2021.

[23] Y. O. Al-Ghamdi, K. A. Alamry, M. A. Hussein, H. M. Marwani, and A. M. Asiri, "Sulfone-modified chitosan as selective adsorbent for the extraction of toxic Hg(II) metal ions," *Adsorption Science & Technology*, vol. 37, no. 1-2, pp. 139–159, 2019.

[24] G. Joo, W. Lee, and Y. Choi, "Heavy metal adsorption capacity of powdered Chlorella vulgaris biosorbent: effect of chemical modification and growth media," *Environmental Science Pollution Ressearch International*, vol. 28, no. 20, pp. 25390–25399, 2021.

[25] M. Descostes, I. Pointeau, J. Radwan et al., "Adsorption and retarded diffusion of EuIII-EDTA− through hard clay rock," *Journal of Hydrology*, vol. 544, pp. 125–132, 2017.

[26] U. C. Yağcıoğlu, T. Bak, and C. Şen, "Bayburt Taşı (Tüfit)," *Mavi Gezegen*, vol. 26, pp. 91–165, 2019.

[27] O. P. Aghamelu, P. N. Nnabo, and H. N. Ezeh, "Geotechnical and environmental problems related to shales in the Abakaliki area, Southeastern Nigeria," *African Journal of Environmental Science and Technology*, vol. 5, no. 2, pp. 80–88, 2010.

[28] M. Arslan, Z. Arslan, and A. Dokuz, "Petrographical, geochemical and petrological characteristics of the Bayburt tuffs: Eocene calk-alkaline felsic volcanism in the southern zone of eastern Pontide," *Secuk University Journal Of Engineering Science And Technology (SUJEST)*, vol. 20, no. 1, pp. 49–68, 2005.

[29] Y. Cao, W. Xiao, G. Shen et al., "Carbonization and ball milling on the enhancement of Pb (II) adsorption by wheat straw: competitive effects of ion exchange and precipitation," *Bioresource Technology*, vol. 273, pp. 70–76, 2019.

[30] M. R. Awual, "Novel conjugated hybrid material for efficient lead(II) capturing from contaminated wastewater," *Materials Science & Engineering C*, vol. 101, pp. 686–695, 2019.

[31] M. R. Awual and M. M. Hasan, "A ligand based innovative composite material for selective lead(II) capturing from wastewater," *Journal of Molecular Liquids*, vol. 294, article 111679, 2019.

[32] V. K. Gupta, S. Agarwal, and T. A. Saleh, "Synthesis and characterization of alumina-coated carbon nanotubes and their application for lead removal," *Journal of Hazardous Materials*, vol. 185, no. 1, pp. 17–23, 2011.

[33] A. A. Taha, M. A. Shreadah, A. M. Ahmed, and H. F. Heiba, "Multi-component adsorption of Pb (II), Cd(II), and Ni(II) onto Egyptian Na-activated bentonite; equilibrium, kinetics, thermodynamics, and application for seawater desalination," *Journal of Environmental Chemical Engineering*, vol. 4, no. 1, pp. 1166–1180, 2016.

[34] L. J. Kennedy, J. J. Vijaya, G. Sekaran, and K. Kayalvizhi, "Equilibrium, kinetic and thermodynamic studies on the adsorption of m-cresol onto micro- and mesoporous carbon," *Journal of Hazardous Materials*, vol. 149, no. 1, pp. 134–143, 2007.

[35] Q. Jiang, W. Xie, S. Han, Y. Wang, and Y. Zhang, "Enhanced adsorption of Pb (II) onto modified hydrochar by polyethyleneimine or H3PO4: an analysis of surface property and interface mechanism," *Colloids and Surfaces A: Physicochemical and Engineering Aspects*, vol. 583, article 123962, 2019.

[36] W. Xu, Y. Song, K. Dai, S. Sun, G. Liu, and J. Yao, "Novel ternary nanohybrids of tetraethylenepentamine and graphene oxide decorated with MnFe2O4 magnetic nanoparticles for the adsorption of Pb (II)," *Journal of Hazardous Materials*, vol. 358, pp. 337–345, 2018.

[37] Y. Qi, J. Wang, X. Wang, J. J. Cheng, and Z. Wen, "Selective adsorption of Pb (II) from aqueous solution using porous biosilica extracted from marine diatom biomass: properties and mechanism," *Applied Surface Science*, vol. 396, pp. 965–977, 2017.

[38] R. Hasan, S. N. Bukhari, R. Jusoh, N. S. A. Mutamin, and H. D. Setiabudi, "Adsorption of Pb(II) onto KCC-1 from aqueous solution: Isotherm and kinetic study," *Materials Today: Proceedings*, vol. 5, no. 10, pp. 21574–21583, 2018.

[39] M. S. Samuel, S. S. Shah, J. Bhattacharya, K. Subramaniam, and N. D. Pradeep Singh, "Adsorption of Pb (II) from aqueous solution using a magnetic chitosan/graphene oxide composite and its toxicity studies," *International Journal of Biological Macromolecules*, vol. 115, pp. 1142–1150, 2018.

[40] Y. Wang, X. Wang, X. Wang et al., "Adsorption of Pb (II) from aqueous solution to Ni-doped bamboo charcoal," *Journal of Industrial and Engineering Chemistry*, vol. 19, no. 1, pp. 353–359, 2013.

[41] N. Al-Jammal, T. Juzsakova, B. Zsirka et al., "Modified Jordanian zeolitic tuff in hydrocarbon removal from surface water," *Journal of Environmental Management*, vol. 239, pp. 333–341, 2019.

[42] K. K. Al-Zboon, B. M. Al-smadi, and S. Al-Khawaldh, "Natural volcanic tuff-based geopolymer for Zn removal: adsorption isotherm, kinetic, and thermodynamic study," *Water, Air, & Soil Pollution*, vol. 227, no. 7, 2016.

[43] P. Pichat, R. Beaumont, and D. Barthomeuf, "Infra-red structural study of aluminium-deficient Y zeolites," *Journal of the Chemical Society, Faraday Transactions 1: Physical Chemistry in Condensed Phases*, vol. 70, pp. 1402–1407, 1974.

[44] M. L. Chavez, L. de Pablo, and T. A. Garcia, "Adsorption of $Ba2^{+}$ by Ca-exchange clinoptilolite tuff and montmorillonite clay," *Journal of Hazardous Materials*, vol. 175, no. 1-3, pp. 216–223, 2010.

[45] S. Jing, M. X. Lan, W. Wen, Z. Jing, Z. Hao, and W. Y. Jun, "Adsorption characteristics of atrazine on different soils in the presence of Cd(II)," *Adsorption Science & Technology*, vol. 38, no. 7-8, pp. 225–239, 2020.

[46] O. Salmani Nuri, M. Irannajad, and A. Mehdilo, "Reagent adsorption on modified mineral surfaces: isotherm, kinetic and thermodynamic aspects," *Journal of Molecular Liquids*, vol. 291, p. 111311, 2019.

[47] K. Vasanth Kumar and S. Sivanesan, "Sorption isotherm for safranin onto rice husk: comparison of linear and non-linear methods," *Dyes and Pigments*, vol. 72, no. 1, pp. 130–133, 2007.

[48] N. A. H. Mohamad Zaidi, L. B. L. Lim, and A. Usman, "Enhancing adsorption of Pb (II) from aqueous solution by NaOH and EDTA modified Artocarpus odoratissimus leaves," *Journal of Environmental Chemical Engineering*, vol. 6, no. 6, pp. 7172–7184, 2018.

[49] H. N. Tran, E. C. Lima, R. Juang, J. C. Bollinger, and H. P. Chao, "Thermodynamic parameters of liquid–phase adsorption process calculated from different equilibrium constants related to adsorption isotherms: a comparison study," *Journal of Environmental Chemical Engineering*, vol. 9, no. 6, article 106674, 2021.

[50] N. Ghasemi, M. Ghasemi, S. Moazeni et al., "Zn (II) removal by amino-functionalized magnetic nanoparticles: kinetics,

isotherm, and thermodynamic aspects of adsorption," *Journal of Industrial and Engineering Chemistry*, vol. 62, pp. 302–310, 2018.

[51] J. Zhang, J. Shao, Q. Jin et al., "Sludge-based biochar activation to enhance Pb (II) adsorption," *Fuel*, vol. 252, pp. 101–108, 2019.

[52] Y. Chu, M. A. Khan, F. Wang, M. Xia, W. Lei, and S. Zhu, "Kinetics and equilibrium isotherms of adsorption of Pb (II) and Cu(II) onto raw and arginine-modified montmorillonite," *Advanced Powder Technology*, vol. 30, no. 5, pp. 1067–1078, 2019.

[53] Q. Gao, X. Wang, H. Wang, D. Liang, J. Zhang, and J. Li, "Sulfhydryl-modified sodium alginate film for lead-ion adsorption," *Materials Letters*, vol. 254, pp. 149–153, 2019.

[54] C. Bai, L. Wang, and Z. Zhu, "Adsorption of Cr(III) and Pb(II) by graphene oxide/alginate hydrogel membrane: Characterization, adsorption kinetics, isotherm and thermodynamics studies," *International Journal of Biological Macromolecules, article inpress*, vol. 147, pp. 898–910, 2020.

[55] Q. Li, L. Chai, Z. Yang, and Q. Wang, "Kinetics and thermodynamics of Pb (II) adsorption onto modified spent grain from aqueous solutions," *Applied Surface Science*, vol. 255, no. 7, pp. 4298–4303, 2009.

[56] F. Wang, J. Li, Y. Su et al., "Adsorption and recycling of Cd(II) from wastewater using straw cellulose hydrogel beads," *Journal of Industrial and Engineering Chemistry*, vol. 80, pp. 361–369, 2019.

[57] M. Lu, Y. Zhang, Y. Zhou et al., "Adsorption-desorption characteristics and mechanisms of Pb (II) on natural vanadium, titanium-bearing magnetite-humic acid magnetic adsorbent," *Powder Technology*, vol. 344, pp. 947–958, 2019.